Bidirectional power flow in an electric vehicle using predictive control algorithm including sneak circuit analysis

Sri Latha Eti[1], Kasibhatla Rama Sudha[1], Molleti Venkata Pankaj Lahari[2], Akkapeddi Chandra Sekhar[3]
[1]Department of Electrical Engineering, Andhra University, Visakhapatnam, India
[2]Department of Electrical and Electronics Engineering, GVP College of Engineering, Visakhapatnam, India
[3]Department of Mathematics, GITAM University, Visakhapatnam, India

Article Info

ABSTRACT

The use of electric vehicle battery chargers is becoming more common for transferring power between grid and energy storage system. This paper focuses on providing a comprehensive understanding of various modes of operation of these battery chargers. Two different controllers are used; one is the predictive power controller at the grid end to generate active and reactive power references to operate a 3-phase AC/DC converter connected between the power grid and the DC link and the other is a hysteresis current controller used to operate a reversible DC/DC converter connected between the DC link and electric vehicle battery and is considered as the main component of the energy storage system. Also, sneak circuit analysis is carried out on the DC/DC converter and the controller is designed accordingly. Results from simulations validate the suggested control scheme's viability and efficacy. The adopted topology is validated in real time with dSpace 1104 hardware in the loop prototype operating in different scenarios, both in steady-state and during transients.
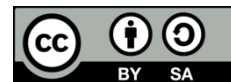
Corresponding Author:

Kasibhatla Rama Sudha
Department of Electrical Engineering, Andhra University
Visakhapatnam, Andhra Pradesh, India
Email: prof.kramasudha@andhrauniversity.edu.in

1. INTRODUCTION

The term "bidirectional power transfer" refers to the mutual exchange of active power between the electric vehicle charger and the power grid. Bidirectional AC-DC converter acts as a crucial component in the energy storage system as it is able to provide a bidirectional power exchange operation and synchronization with the grid. It tackles with power quality issues caused by high harmonic distortions (THD), low power factor issues, voltage alterations, DC voltage and current ripples [1]. Therefore, the AC-DC converter control algorithm must be effective and stable.

To obtain an improved efficiency and usefulness of the bidirectional AC-DC converter, several studies have been carried out. The mostly preferred technique is a linear voltage-control technique (VCT) which employs linear proportional integral derivative (PID) controllers and a space vector modulation scheme (SVM) to control the power flow indirectly using the active component and reactive component of grid currents [2]. Using coordinate transformation, the observed grid AC currents are converted into active currents and reactive currents, which are described in the α-β coordinates [3], [4]. The SVM technique generates a switching sequence for insulated gate bipolar transistor (IGBTs) in every sampling period so that the average output voltage of the 3-Φ AC-DC converter is proportional to the signals obtained from the controllers making it operate with a fixed switching frequency at a pre-defined sampling time [5].

The bidirectional battery charger's entire electrical diagram is displayed in Figure 1. The charging/discharging currents and the active/reactive power supplied by the power grid and electric vehicles, respectively, should be tracked by the bidirectional chargers. Taking the nominal battery voltage of 300 V into consideration, a 3-Φ AC/DC bidirectional converter circuit, is chosen at the rectification stage with a 100 V three phase supply voltage [6]. It is connected to the AC supply mains in series with 'line resistance (R_a)' and 'line inductance (L_a)'. A capacitor (C_{dc}) is connected at the output terminals of the converter to provide a smooth DC output voltage. Reversible DC-DC converter is connected in the second stage, to which an output inductance (L_{dc}) and the electric vehicle battery are connected [7]–[10].
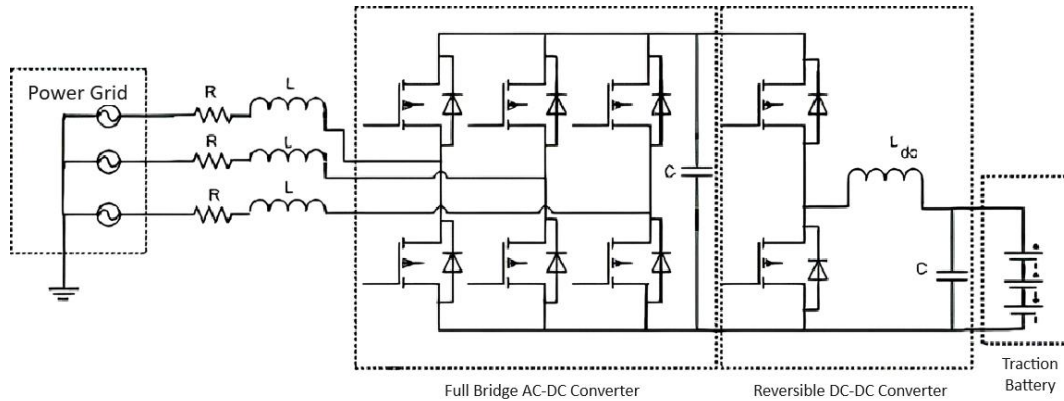

Figure 1. Grid connected bi-directional converter and reversible DC - DC converter circuit

In this paper, the description of the circuits and system operation of the 3-Φ bidirectional AC-DC rectifier and reversible DC-DC converter are explained in section 2. The sneak circuit analysis is carried out and the proper switching control sequence for the DC-DC converter is obtained in section 3, followed by section 4, where the controllers for the AC-DC rectifier and the DC-DC converter is explained. Simulation results were presented in section 5 and a detailed explanation is presented for the results obtained. Conclusion of the paper is provided in section 6 followed by bibliography.

2. DESCRIPTION OF CIRCUIT AND SYSTEM OPERATION
2.1. 3-Φ AC–DC converter
The 3-Φ bidirectional AC-DC converter topology shown in Figure 2 illustrates the power transfer between the grid and the DC bus. Six IGBT switches (S1–S6) form the bidirectional AC–DC converter is connected to the power grid using line inductance (L_a) in series with line resistance (R_a). In order to stabilize the DC bus voltage (V_{dc}), a capacitor (C_{dc}) is placed at the DC link to filter ripples in the output DC voltage [11]–[13]. The bidirectional AC-DC converter has two operating modes. In the first operating mode, which is also called as the rectifier mode, it enables power transfer from 3-Φ source to the DC link. In the second operating mode, also called as the inverter mode, the power flows from the DC link to the 3-Φ voltage terminals.

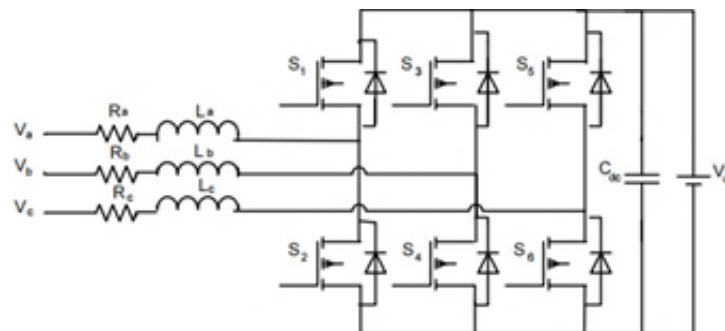Figure 2. 3-Φ bidirectional AC–DC converter circuit

Using the electrical system depicted in Figure 2, the power circuit for the 3-Φ bidirectional AC-DC converter transforms electrical energy from AC and DC form. Two switches are connected in each leg of the converter, which must operate in complimentary mode to prevent short circuits. As a result, the switching states of the 3-Φ bidirectional AC-DC converter can be obtained from the three gating signals namely, S_a, S_b, and S_c and can be defined as (1)-(4) [14]. The switching signals are defined as (1).

$$S_K = \begin{cases} 1; S_1/S_3/S_5 - \text{ON} \\ 0; S_2/S_4/S_6 - \text{OFF} \end{cases} \tag{1}$$

Thus, the switching vector (S_K) can be expressed as (2) [15].

$$\begin{bmatrix} S_\alpha \\ S_\beta \end{bmatrix} = \frac{2}{3} \begin{bmatrix} 1 & -\frac{1}{2} & -\frac{1}{2} \\ 0 & \frac{\sqrt{3}}{2} & -\frac{\sqrt{3}}{2} \end{bmatrix} \begin{bmatrix} S_a \\ S_b \\ S_c \end{bmatrix} \tag{2}$$

Here, α-β coordinates are used for simplification of the analysis of 3-Φ circuits. The 3-Φ voltages (V_a, V_b, V_c) are expressed in the α-β coordinates similar to (2) as (3).

$$\begin{bmatrix} V_\alpha \\ V_\beta \end{bmatrix} = \frac{2}{3} \begin{bmatrix} 1 & -\frac{1}{2} & -\frac{1}{2} \\ 0 & \frac{\sqrt{3}}{2} & -\frac{\sqrt{3}}{2} \end{bmatrix} \begin{bmatrix} V_a \\ V_b \\ V_c \end{bmatrix} \tag{3}$$

In terms of switching states, the voltage vector can be expressed as (4).

$$\begin{bmatrix} V_\alpha \\ V_\beta \end{bmatrix} = \begin{bmatrix} S_\alpha \\ S_\beta \end{bmatrix} \times V_{dc} \tag{4}$$

Where, V_{dc} - the DC output voltage obtained from the converter.

The six valid switching states are presented in the Table 1. The switching states 0/0/0 and 1/1/1 are avoided for safety as the three phases are never turned on at the same time. The average power output in all the six switching states is 2 Vdc/3. The power flow equations from grid side to output in α-β coordinates are as (5).

$$L \frac{di_{g\alpha\beta}}{dt} = V_{g\alpha\beta} - Ri_{g\alpha\beta} - V_{\alpha\beta} \tag{5}$$

Where, Vgαβ and igαβ indicate the grid side voltage and current. The derivative of current obtained from the Euler's approximation in expanded form is written as (6).

$$\frac{di_{g\alpha\beta}}{dt} = \frac{i_{g\alpha\beta}(k+1) - i_{g\alpha\beta}(k)}{T_s} \tag{6}$$

On substitution into (5) and simplifying as (7).

$$\frac{i_{g\alpha\beta}(k+1) - i_{g\alpha\beta}(k)}{T_s} = \frac{1}{L} \left[V_{g\alpha\beta}(k) - Ri_{g\alpha\beta}(k) - V_{\alpha\beta}(k) \right] \tag{7}$$

$$i_{g\alpha\beta}(k+1) = \frac{T_s}{L} \left[V_{g\alpha\beta}(k) - Ri_{g\alpha\beta}(k) - V_{\alpha\beta}(k) \right] + i_{g\alpha\beta} \tag{8}$$

The 3-Φ grid currents in the standard α-β coordinates for the next time instant shown in (8). Thus, the expressions for the active power and the reactive power for the time instant (k+1) are calculated as (9).

$$P(k+1) = \frac{3}{2} \text{Re} \left[V_{g\alpha\beta}(k+1) * i_{g\alpha\beta}^*(k+1) \right] \tag{9}$$

$$P(k+1) = \frac{3}{2} \left[V_{g\alpha}(k+1) * i_{g\alpha}(k+1) + V_{g\beta}(k+1) * i_{g\beta}(k+1) \right] \tag{10}$$

Here in (11) and (12), $V_{g\alpha\beta}(k+1)$ represents the predicted values of grid voltages for the time instant (k+1) and are approximated to the measured values $V_{g\alpha\beta}(k)$.

$$V_{g\alpha}(k+1) \cong V_{g\alpha}(k) \; ; \; V_{g\beta}(k+1) \cong V_{g\beta}(k) \tag{11}$$

$$P(k+1) = \frac{3}{2} \left[V_{g\alpha}(k) \, i_{g\alpha}(k+1) + V_{g\beta}(k) \, i_{g\beta}(k+1) \right] \tag{12}$$

In the same way, the reactive power equation can be expressed as (13) and (14).

$$Q(k+1) = \frac{3}{2} \, \text{Img}\big[V_{g\alpha\beta}(k+1) \, i_{g\alpha\beta}^{*}(k+1)\big] \tag{13}$$

$$Q(k+1) = \frac{3}{2} \big[V_{g\beta}(k) \, i_{g\alpha}(k+1) - V_{g\alpha}(k) \, i_{g\beta}(k+1)\big] \tag{14}$$

According to the needs of the grid and the consumers, switching pulses to the converter can be obtained using the predicted values of the active and reactive power.

Table 1. Switching states of bidirectional AC–DC converter in α - β coordinates

Switching states in 3-Φ coordinates			Switching states in α-β coordinates		Voltages in α-β coordinates	
S_a	S_b	S_c	S_α	S_β	V_α	V_β
0	0	1	-1/3	-1/√3	$-V_{dc}/3$	$-V_{dc}/\sqrt{3}$
0	1	0	-1/3	1/√3	$-V_{dc}/3$	$V_{dc}/\sqrt{3}$
0	1	1	-2/3	0	$-2V_{dc}/3$	0
1	0	0	2/3	0	$2V_{dc}/3$	0
1	0	1	1/3	-1/√3	$V_{dc}/3$	$-V_{dc}/\sqrt{3}$
1	1	0	1/3	1/√3	$V_{dc}/3$	$V_{dc}/\sqrt{3}$

2.2. Reversible DC–DC converter

Basically, DC-DC converters are useful for converting voltages to higher or lower levels depending on the circuit operation and requirement. Reversible DC-DC converter in this case are particularly used to charge the electric vehicle batteries [16]. The electric vehicle battery charger is assumed to be charging lithium ion batteries with a nominal voltage of 300 V. The DC-DC converter regulates the battery current (i_{bat}) and voltage of the battery cells at their nominal ranges.

The voltage and current relations of the DC-DC converter and battery cells can be determined from Figure 3 as (15).

$$V_{dc} = L_{dc} \frac{di_{bat}}{dt} + V_{bat} \tag{15}$$

Where, V_{dc} is the DC link voltage; V_{bat}, and i_{bat} are the voltage of the battery and the current passing through the inductor L_{dc}, respectively. On simplification, (15) can be rewritten as (16).

$$\frac{di_{bat}}{dt} = \frac{1}{L_{dc}} [V_{dc} - V_{bat}] \tag{16}$$

From Euler's approximation, the battery current can be represented for the time instant (k+1) as (17).

$$\frac{i_{bat}(k+1) - i_{bat}(k)}{T_s} = \frac{1}{L_{dc}} [V_{dc} - V_{bat}] \tag{17}$$

The (18) will be useful in controlling the operation of reversible DC-DC converter by comparison of the upcoming current value with the reference current value. It also regulates the voltage (V_{bat}) required for charging the batteries.

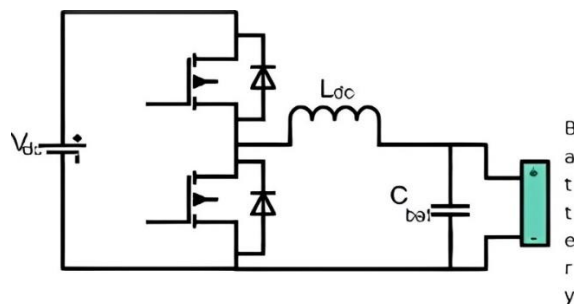$$i_{bat}(k+1) = \frac{T_s}{L_{dc}} [V_{dc} - V_{bat}] + i_{bat}(k) \tag{18}$$

Figure 3. Reversible DC–DC converter circuit

3. SNEAK CIRCUIT ANALYSIS OF DC-DC CONVERTER

In general, a power converter has several operating stages and can be switched using the control technique. Because every operating stage corresponds to a sub circuit, a current flow through an unexpected path causes undesired results in certain conditions called sneak current paths [17]. Therefore, sneak circuit analysis is a must in power converters for eliminating these unexpected paths by proper control strategy or changes in topology. To find the sneak current paths in the DC–DC converter shown in Figure 4(a), a directed graph is established using graph theory. All the branches of the converter are called as edges; the node representing the intersection of two or more branches is called as vertex; the component connected in the branch is the name of edge; the current flow direction through the component in a branch is the edge direction [18], [19]. Thus, the directed graph of the DC-DC converter obtained from the above method is shown in Figure 4(b).

From the definition of the adjacency matrix [17], for the DC–DC converter of the network graph in Figure 4(b) can be obtained as (19).

$$A = \begin{bmatrix} 0 & 1 & 0 & 1 \\ 1 & 0 & 1 & 1 \\ 0 & 1 & 0 & 1 \\ 1 & 1 & 1 & 0 \end{bmatrix} \tag{19}$$

The connection matrix elements can be defined as (20).

$$c_{ij} = \begin{cases} 1; \text{for } i = j \\ 0; \text{for } i \neq j \text{ and no cuurent path from i to j} \\ \text{Symbol of the element; for } i \neq j \end{cases} \tag{20}$$

As a result, the generalized DC-DC converter connection matrix can be written as (21).

$$c = \begin{matrix} 1 & G_1 & 0 & V_{dc} \\ G_1 & 1 & L_{dc} & G_2 \\ 0 & L_{dc} & 1 & C_b + R \\ V_{dc} & G_2 & C_b + R & 1 \end{matrix} \tag{21}$$

Since, the current always flows in a loop in the circuit, it is possible to identify every potential current loop in the converter by computing the determinant of matrix C [18], [19].

$$\begin{aligned} |DetC| = {} & 1 - C_b^2 - R^2 - 2RC_b - L_{dc}^2 + L_{dc}C_bG_2 + L_{dc}G_2R - G_2^2 + G_1^2 - G_1^2C_b^2 - G_1^2R^2 \\ & -2G_1C_bR + G_1V_{dc}L_{dc}C_b + G_1V_{dc}L_{dc}R - G_1G_2V_{dc} - G_1V_{dc}L_{dc}C_b - V_{dc}G_1L_{dc}R \\ & +C_{dc}G_1G_2 - C_{dc}^2 + C_{dc}^2L_{dc}^2 \end{aligned}$$

From the above equation, loops having both switches G1 and G2 can be avoided as both switches do not urn on simultaneously. Quadratic terms are also avoided as they don't make any sense [20]. Thus, from the equation (22), it is clear that the circuit consists of 5 valid current paths. Out of these five paths, the desired current paths are as in (23).

$$|DetC| = C_bR + L_{dc}G_2C_b + L_{dc}G_2R + V_{dc}G_1L_{dc}C_b + V_{dc}G_1L_{dc}R \tag{22}$$

$$\begin{aligned} V_{dc} - G_1 - L_{dc} - R \\ R - L_{dc} - G_2 \end{aligned} \tag{23}$$

To find the operating stages of the circuit, the possible sub - circuits for each current path are identified using Mesh Analysis. From the circuit shown in Figure 4(a), the three meshes are represented as (24).

$$\begin{aligned} M_1 &= \{V_{dc}, G_1, G_2\} \\ M_2 &= \{G_2, L_{dc}, C_b\} \\ M_3 &= \{C_b, R\} \end{aligned} \tag{24}$$

On application of and (∪) operation and ring sum (⊕) operation of the graph theory, the three possible mesh circuits can be identified as (25).

$$M_2 \cup M_3 = \{G_2, L_{dc}, R\}$$
$$M_2 \oplus M_3 = \{G_2, L_{dc}, C_b, R\}$$
$$M_1 \cup M_2 \oplus M_3 = \{V_{dc}, G_1, G_2, C_b, R\}$$
$$M_3 = \{C_b, R\} \tag{25}$$

It can be observed from the above (25) that $M_2 \oplus M_3, M_1 \cup M_2, \oplus M_3, and M_3$ represent the three operating stages. Therefore, the possible paths for current flow in the converter, meshes and the operating stages are obtained. Now, the behavior of the converter during the presence of sneak circuit paths while operating need to be determined by carrying out sneak circuit analysis. In general, the switching components G_1 and G_2 are turned 'ON' and turned 'OFF' in a pre-determined order according to the control strategy. Therefore, the operating modes of the DC-DC converter will consist of the sub-circuits corresponding to various switching states [21].

Let '1' be ON state of the switches G_1 and G_2 and '0' indicate their OFF state. Then, the possible switching states that are valid can be expressed as (26).

$$G_1 G_2 = 1\ 0$$
$$G_1 G_2 = 0\ 1$$
$$G_1 G_2 = 0\ 0 \tag{26}$$

The switching state $G_1 G_2 = 1\ 1$ is invalid as both the switches are always operated as conjugates. Thus, the three valid switching states constitute two switching sequences:
- Control sequence I comprise of switching sequence, as in (27).

$$G_1 G_2 = 1\ 0\ ;\ 0\ 1\ ;\ 1\ 0\ ;\ 0\ 1\ ;\ 1\ 0\ ;\ 0\ 1; \tag{27}$$

- Control sequence II comprises of switching sequence, as in (28).

$$G_1 G_2 = 1\ 0\ ;\ 0\ 1\ ;\ 0\ 0\ ;\ 1\ 0\ ;\ 0\ 1\ ;\ 0\ 0\ ;\ 1\ 0\ ;\ 0\ 1;\ 0\ 0; \tag{28}$$
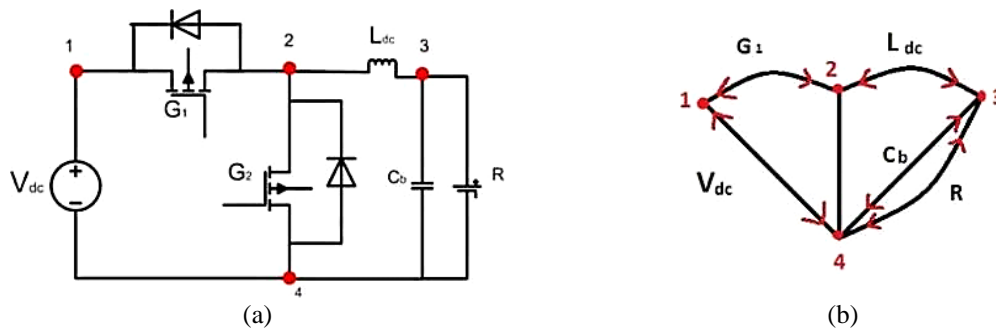

(a)　　　　　　　　　　　　　(b)

Figure 4. Representing a DC-DC converter circuit (a) with nodes and (b) as a directed network graph

The equivalent circuits corresponding to each switching state as indicated by (26) are depicted by the Figures 5(a)-5(d), respectively. Thus, the operating modes under control sequence I represented by (27) are shown in above Figures 5(a) and 5(b) and are considered as normal operating modes. The operating modes under control sequence II represented by (28) have two different paths for current and are assumed to be the sneak operating modes and can be observed in Figure 6 and Figure 7, respectively.

Due to these sneak operating paths, the number of operating stages increases which leads to energy imbalance and the desired performance characteristics of the converter gets disturbed. To eliminate these sneak operating modes, any of the following mentioned ways can be implemented: i) Proper selection of control sequence; ii) Proper parameter design; and iii) Topology modification. In this paper, proper selection of control sequence method is followed. Thus, the control sequence I is chosen to avoid sneak circuit paths occurring during the operation of DC-DC converter.
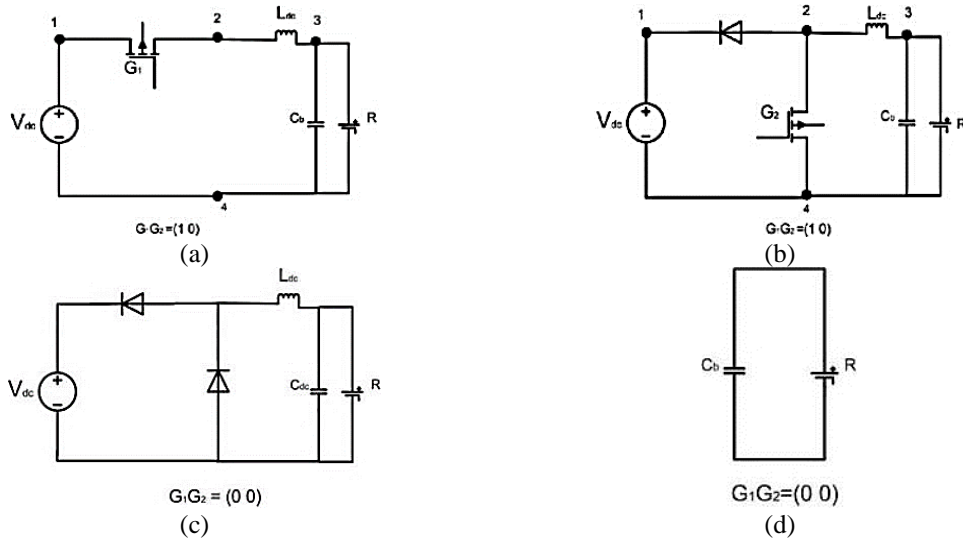
Figure 5. Equivalent circuit of the DC- DC converter for: (a) switching state G1G2 = 1 0, (b) switching state G1G2 = 0 1, (c) switching state G1G2 = 0 0, and (d) switching state G1G2 = 0 0
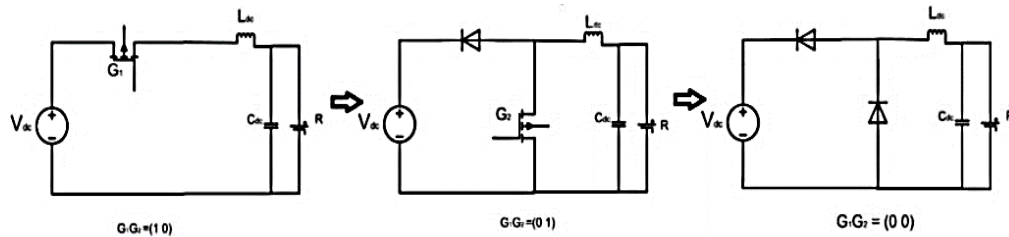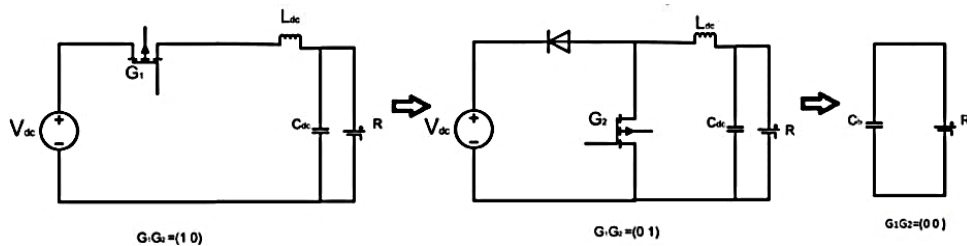

Figure 6. Sneak operating path I

Figure 7. Sneak operating path II

4. CONTROLLER STRUCTURE AND DESIGN CONSIDERATIONS
4.1. Predictive control technique for bidirectional AC-DC converter

In general, the conventional predictive control technique is a current control technique, in which, the output current continuously tracks its reference value by using the discrete behavior of the converter. Figure 8 shows the predictive control technique for the 3-Φ bidirectional AC–DC converter. In this circuit, the grid current and grid voltage are transformed into the standard α-β coordinates using (3). The six switching pulses, obtained from Table 1 are used to calculate the reference voltage values [22]. The predictive grid current in α-β coordinates for (k+1) instant is obtained from (8) and the instantaneously changing values of active and reactive power for time instant (k+1) are calculated using (12) and (14).

The command of the reference active power (Pref) is determined from the reference battery current signal using (29).

$$P_{ref} = V_{bat} \times i^*_{batref} \tag{29}$$

The reference reactive power command Q_{ref} is a presumed signal which implies the different stages of power flow in the system. Depending on changes in magnitude and sign convention of instantaneous active power

and reactive power values, the most suitable switching state of the converter for complete control of active power and reactive power during each and every sector is chosen [23], [24]. The error signals obtained from (30) which gives the minimal error and the instant which provides the minimal error is chosen to be the next switching instant to the bidirectional rectifier.

$$\Delta S = \sqrt{(P(k+1) - P_{ref})^2 + (Q(k+1) - Q_{ref})^2} \tag{30}$$

4.2. Hysteresis current control

The control circuitry for reversible DC–DC converter is represented in Figure 9. in which the predictive battery current is calculated using (18). The gating pulses to IGBT 1 and IGBT 2 are generated from the hysteresis current controller taking the battery reference current and comparing with the current obtained for the (k+1) instant. When the battery current for the (k+1) instant is more than the battery reference current, the error will be more than the upper hysteresis limit and IGBT G1 is triggered. In that case, the DC–DC Converter works as a buck converter and the battery of the electric vehicle is in charging mode. When the battery current for the (k+1) instant is less than the battery reference current, the error will be less than the lower hysteresis limit and IGBT G2 is triggered. In this case, the DC–DC converter works as a boost converter and the battery of the electric vehicle is in discharging mode and supplies the grid [25].
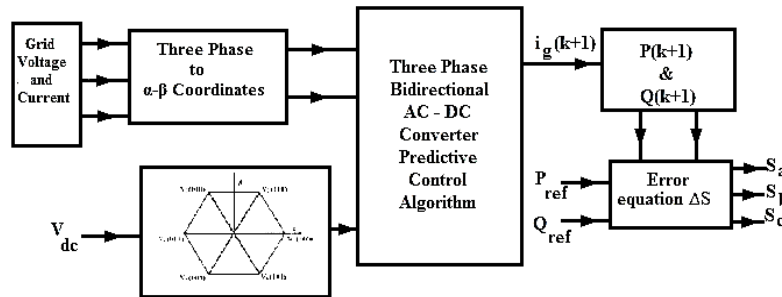

Figure 8. Predictive control technique for 3-Φ bidirectional AC–DC converter
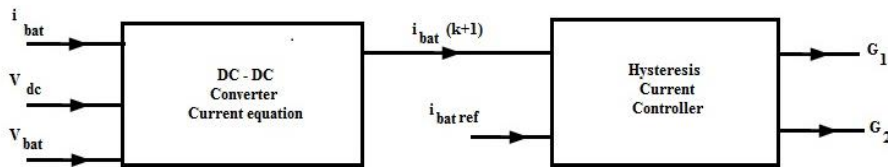

Figure 9. Control circuit for reversible DC-DC waveform

5. SIMULATION ANALYSIS

Simulation results are obtained from MATLAB/Simulink R2019a and are presented in this section. Also, the results obtained from dSpace DS1104 control board connected to host computer with MATLAB/Simulink installed in it and hardware in the loop interface were presented in the below section which provides the real time validation of the system under consideration. The specifications of the system represented in Figure 1 are provided in the Table 2.

Table 2. Model parameters chosen in simulation

Parameter	Value
Per phase line resistance (R_a) in Ohms	0.25
Per phase line inductance (L_a) in Henry	10×10^{-3}
DC capacitor (C_{dc}) in Farads	550×10^{-6}
DC inductor at output terminals (L_{dc}) in Henry	100×10^{-3}
Battery capacitor (C_{bat}) in Farads	750×10^{-6}
Line to line voltage at grid (V_g) in volts	100
Supply frequency in Hertz	50
Battery voltage (V_{bat}) in Volts	300
Sampling frequency (f_s) in Hertz	20×10^3

The reference battery charging current (i_{batref}) is initially maintained at 6.675 A, the battery voltage is maintained at 299.2 V which can be observed in Figures 10(a) and 10(b) respectively. During this period, the active power reference (P_{ref}) is maintained at 2 KW and the reactive power reference (Q_{ref}) is maintained at 0 KVar which can be observed in Figures 11(a) and 11(b) respectively. At t= 1 sec, the battery reference current is stepped down to -6.675 A, which declines the active power reference value to -2 KW. The battery reference current is made 0 at t=2 sec, which makes the active power reference to trace 0 KW at t=2 sec. The battery current reference is again increased to 6.675 A at t=4 sec, which raises the active power reference command to 2 KW.
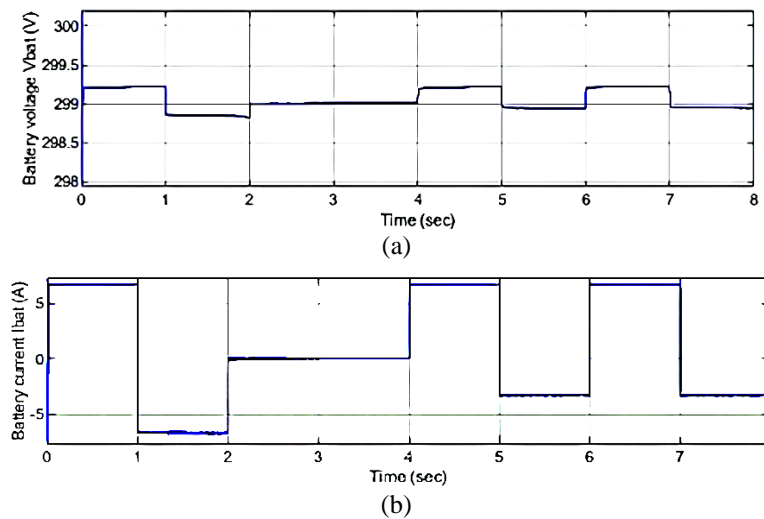
Figure 10. Output waveforms of (a) battery voltage and (b) battery current

The reactive power reference command also is raised to +1 KVar at this instant. The battery reference current is reduced to -3.33 A at t=5 sec, there is a voltage drop by a small value at this instant. The active power command falls to -1KW and reactive power command is maintained at +1 KVar during this period from t= 5 to 6 sec. The battery current reference is raised to 6.675 A at t=6 sec, when the reference reactive power command is reduced to -1KVar. Again, at t=7 sec, the battery current reference command is reduced to -3.33 A, which reduces the active power command to -1 KW and battery voltage drops by a small value.

For simplicity, the simulation results of the per phase voltage in 'a' phase of the grid and the three-phase currents are presented at different intervals separately. The observations from the simulation results shown in Figures 12(a)-12(g) can be tabulated during different intervals of time as in Table 3, and inferences can be drawn according to the observations.

With MATLAB/Simulink installed in a personal computer serving as a host and a dSpace 1104 control board, the below results have been obtained as in Figure 13. This technique is applied over sample duration of 5ms. The results are obtained for two modes of operation of the system model and the three-phase voltage and current waveform are observed. From the Figure 13, it is observed that the voltage and current waveform are in-phase until t=2 sec, which implies that the battery is charging from supply. After t=2 sec, the three-phase voltages are lagging behind the currents indicating that the battery is supplying power to the supply mains.
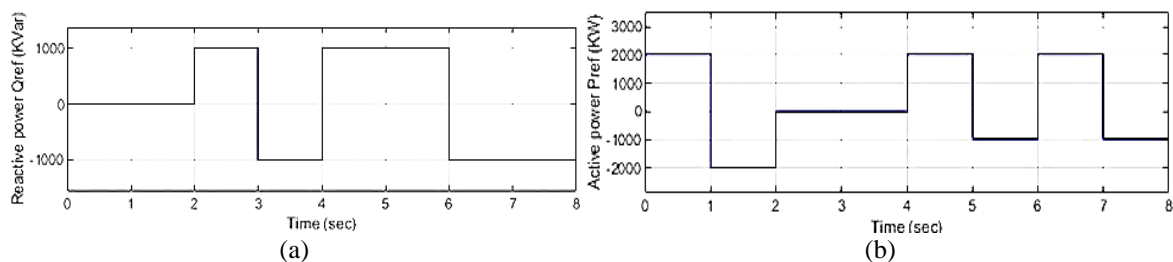

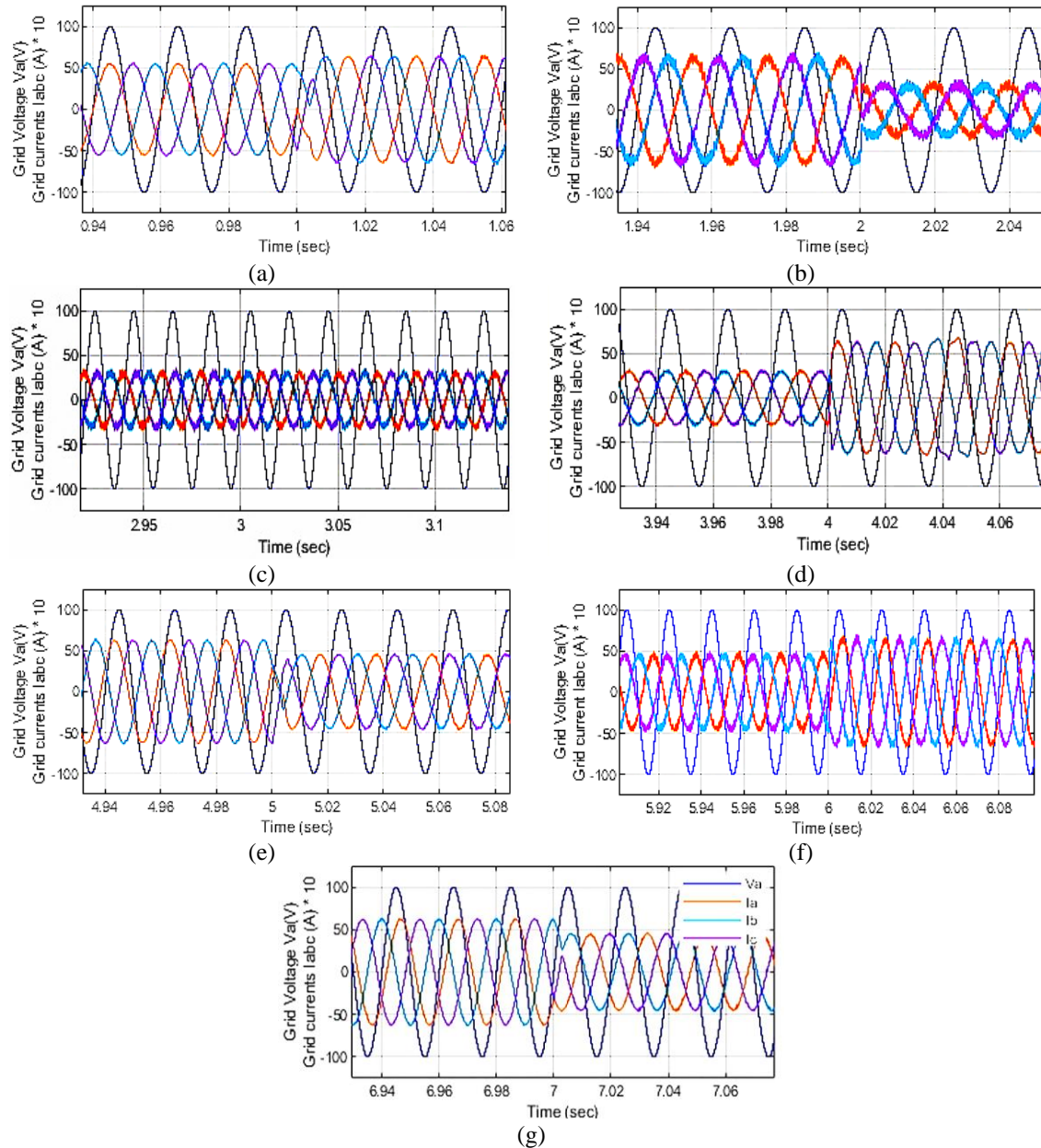Figure 11. Reference command signals: (a) active power and (b) reactive power

Figure 12. Per phase Voltage V_{ga} and 3-Φ Currents I_{gabc}*10 of power grid: (a) during time interval 0<t<1, (b) during time interval 1<t<2, (c) during time interval 2<t<3, (d) during time interval 3<t<4, (e) during time interval 4<t<5, (f) during time interval 5<t<6, and (g) during time interval 6<t<7

Table 3. Observations from grid voltage and current waveforms

| Time interval in sec	Grid voltage V_{ga} (V) & grid currents I_{gabc} (A)*10	Observations
0<t<1	V_{ga} & I_{ga} are in phase	The EV battery charges from grid supply
1<t<2	V_{ga} & I_{ga} are in phase opposition	The EV supplies active power to the grid
2<t<3	I_{ga} is leading V_{ga} by 90⁰	The converter provides reactive power compensation to the grid.
3<t<4	I_{ga} is lagging V_{ga} by 90⁰	The grid supplies reactive power to load
4<t<5	I_{ga} is leading V_{ga}	The power grid supplies load with both positive active and reactive power.
5<t<6	I_{ga} is lagging V_{ga}	The power grid receives active power from the battery.
6<t<7	I_{ga} is lagging V_{ga}	The system works as Static VAR compensator and battery is charged from grid
t>7	I_{ga} is lagging V_{ga}	The system works as Static VAR compensator and battery delivers active power to grid
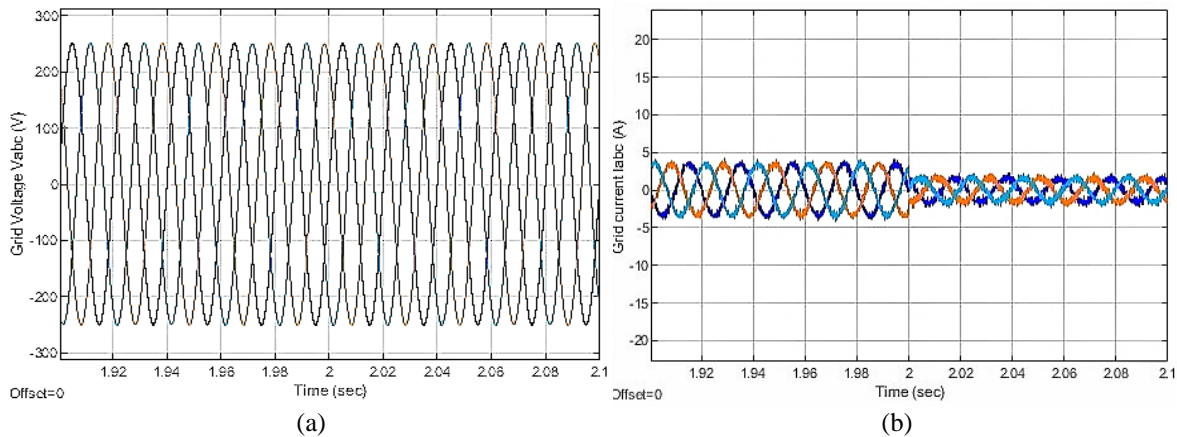
Figure 13. Results obtained from dSpace DS 1104 control board using hardware in the loop mode:
(a) three phase voltages and (b) three phase currents

6. CONCLUSION

The proposed predictive control algorithm in this paper aims to transfer power between the grid and the DC link in energy storage systems. The controller receives active power commands from the customer and reactive power commands from the utility, adjusting the line current and battery charging or discharging current accordingly to meet the demands. Also, the battery of the electric vehicle remains unaffected by the reactive power operation. The simulation results demonstrate fast dynamic response and excellent steady-state performance. To validate the system in real-time, the dSpace 1104 control board is connected to a standalone personal computer with MATLAB installed, operating in hardware in the loop mode.

REFERENCES

[1]   B. Devi and V. S. Kumar, "Lithium-ion battery management system: a review," in *2022 International Conference on Power, Energy, Control and Transmission Systems (ICPECTS)*, Dec. 2022, pp. 1–6. doi: 10.1109/ICPECTS56089.2022.10047494.
[2]   S. Shete, P. Jog, R. K. Kumawat, and D. K. Palwalia, "Battery management system for SOC estimation of lithium-ion battery in electric vehicle: a review," in *2021 6th IEEE International Conference on Recent Advances and Innovations in Engineering (ICRAIE)*, Dec. 2021, pp. 1–4. doi: 10.1109/ICRAIE52900.2021.9703752.
[3]   T. He, D. D.-C. Lu, M. Wu, Q. Yang, T. Li, and Q. Liu, "Four-quadrant operations of bidirectional chargers for electric vehicles in smart car parks: G2V, V2G, and V4G," *Energies*, vol. 14, no. 1, p. 181, Dec. 2020, doi: 10.3390/en14010181.
[4]   S. Kouro, P. Cortes, R. Vargas, U. Ammann, and J. Rodriguez, "Model predictive control—a simple and powerful method to control power converters," *IEEE Transactions on Industrial Electronics*, vol. 56, no. 6, pp. 1826–1838, Jun. 2009, doi: 10.1109/TIE.2008.2008349.
[5]   V. Monteiro, J. G. Pinto, and J. L. Afonso, "Operation modes for the electric vehicle in smart grids and smart homes: present and proposed modes," *IEEE Transactions on Vehicular Technology*, vol. 65, no. 3, pp. 1007–1020, Mar. 2016, doi: 10.1109/TVT.2015.2481005.
[6]   Y. Zhang, W. Xie, Z. Li, and Y. Zhang, "Model predictive direct power control of a PWM rectifier with duty cycle optimization," *IEEE Transactions on Power Electronics*, vol. 28, no. 11, pp. 5343–5351, Nov. 2013, doi: 10.1109/TPEL.2013.2243846.
[7]   A. Bouafia, J.-P. Gaubert, and F. Krim, "Analysis and design of new switching table for direct power control of three-phase PWM rectifier," in *2008 13th International Power Electronics and Motion Control Conference*, Sep. 2008, pp. 703–709. doi: 10.1109/EPEPEMC.2008.4635347.
[8]   A. Calle-Prado, S. Alepuz, J. Bordonau, J. Nicolas-Apruzzese, P. Cortes, and J. Rodriguez, "Model predictive current control of grid-connected neutral-point-clamped converters to meet low-voltage ride-through requirements," *IEEE Transactions on Industrial Electronics*, vol. 62, no. 3, pp. 1503–1514, Mar. 2015, doi: 10.1109/TIE.2014.2364459.
[9]   A. K. Ali and R. G. Omar, "Finite control set model predictive direct current control strategy with constraints applying to drive three-phase induction motor," *International Journal of Electrical and Computer Engineering (IJECE)*, vol. 11, no. 4, pp. 2916–2924, Aug. 2021, doi: 10.11591/ijece.v11i4.pp2916-2924.
[10]   L. E. Jumaa Alkurawy and K. G. Mohammed, "Model predictive control of magnetic levitation system," *International Journal of Electrical and Computer Engineering (IJECE)*, vol. 10, no. 6, pp. 5802–5812, Dec. 2020, doi: 10.11591/ijece.v10i6.pp5802-5812.
[11]   S. K. Dube, R. Nair, and P. Das, "Analysis and design of an integrated bidirectional three-phase AC–DC resonant converter," *IEEE Transactions on Industrial Electronics*, vol. 70, no. 5, pp. 4369–4379, May 2023, doi: 10.1109/TIE.2022.3183274.
[12]   T. Noguchi, H. Tomiki, S. Kondo, and I. Takahashi, "Direct power control of PWM converter without power-source voltage sensors," *IEEE Transactions on Industry Applications*, vol. 34, no. 3, pp. 473–479, 1998, doi: 10.1109/28.673716.
[13]   M. Kesler, M. C. Kisacikoglu, and L. M. Tolbert, "Vehicle-to-grid reactive power operation using plug-in electric vehicle bidirectional offboard charger," *IEEE Transactions on Industrial Electronics*, vol. 61, no. 12, pp. 6778–6784, Dec. 2014, doi: 10.1109/TIE.2014.2314065.
[14]   L. Pan and C. Zhang, "Model predictive control of a single-phase PWM rectifier for electric vehicle charger," *Energy Procedia*, vol. 105, pp. 4027–4033, May 2017, doi: 10.1016/j.egypro.2017.03.850.
[15]   J. G. Pinto *et al.*, "Bidirectional battery charger with grid-to-vehicle, vehicle-to-grid and vehicle-to-home technologies," in *IECON 2013 - 39th Annual Conference of the IEEE Industrial Electronics Society*, Nov. 2013, pp. 5934–5939. doi: 10.1109/IECON.2013.6700108.
[16]   H. Tao, G. Zhang, and Z. Zheng, "Onboard charging DC/DC converter of electric vehicle based on synchronous rectification and characteristic analysis," *Journal of Advanced Transportation*, vol. 2019, pp. 1–10, Jun. 2019, doi: 10.1155/2019/2613893.

[17] M. P. Kazmierkowski, M. Jasinski, and G. Wrona, "DSP-based control of grid-connected power converters operating under grid distortions," *IEEE Transactions on Industrial Informatics*, vol. 7, no. 2, pp. 204–211, May 2011, doi: 10.1109/TII.2011.2134856.

[18] B. Zhang and D. Qiu, "Sneak circuits in power converters: concept, principle and application," *CPSS Transactions on Power Electronics and Applications*, vol. 2, no. 1, pp. 68–75, Apr. 2017, doi: 10.24295/CPSSTPEA.2017.00008.

[19] W. K. Chen and C. Satyanarayana, "Applied graph theory: graphs and electrical networks," *IEEE Transactions on Systems, Man, and Cybernetics*, vol. 8, no. 5, pp. 418–418, 1978, doi: 10.1109/TSMC.1978.4309987.

[20] D. C. Osborn, "Sneak paths in X-Y matrix arrays," *IEEE Journal of Solid-State Circuits*, vol. 4, no. 6, pp. 312–317, Dec. 1969, doi: 10.1109/JSSC.1969.1050029.

[21] S.-Z. Chen, Y. Wang, G. Zhang, L. Chang, and Y. Zhang, "Sneak circuit theory based approach to avoiding short-circuit paths in reconfigurable battery systems," *IEEE Transactions on Industrial Electronics*, vol. 68, no. 12, pp. 12353–12363, Dec. 2021, doi: 10.1109/TIE.2020.3044805.

[22] J. Li, D. Qiu, and B. Zhang, "Sneak circuit analysis for n-stage resonant switched capacitor converters based on graph theory," in *IECON 2007 - 33rd Annual Conference of the IEEE Industrial Electronics Society*, 2007, pp. 1581–1585. doi: 10.1109/IECON.2007.4460006.

[23] F. Senani, A. Rahab, F. Louar, F. Bourourou, and H. Benalla, "Active and reactive power control of DFIG using PI and DPC controllers," in *2015 4th International Conference on Electrical Engineering (ICEE)*, Dec. 2015, pp. 1–6. doi: 10.1109/INTEE.2015.7416841.

[24] Z. Tao and L. Li, "Control loop design and bidirectional control strategy of a bidirectional DC/DC converter," in *IECON 2017 - 43rd Annual Conference of the IEEE Industrial Electronics Society*, Oct. 2017, pp. 5720–5725. doi: 10.1109/IECON.2017.8216992.

[25] W. Yu, H. Qian, and J.-S. Lai, "Design of high-efficiency bidirectional DC–DC converter and high-precision efficiency measurement," *IEEE Transactions on Power Electronics*, vol. 25, no. 3, pp. 650–658, Mar. 2010, doi: 10.1109/TPEL.2009.2034265.

BIOGRAPHIES OF AUTHORS

Sri Latha Eti received B.Tech degree from JNTU Hyderabad, India in 2008 and M.E. degree in power electronics and drives from Andhra University, India in 2015. She is currently pursuing Ph.D. from Andhra University, Visakhapatnam, India. She works as an assistant professor in WISTM Engineering College, Visakhapatnam, India. She has 11 years teaching experience and has published eight papers in international journals. Her areas of interest include power electronic drives, electric vehicle battery charger design, and sneak circuits analysis of DC-DC converters. She can be contacted at email: etisrilatha@gmail.com.

Kasibhatla Rama Sudha received B.E degree from GITAM University, India in 1991 and M.E degree in power systems from Andhra University, India in 1994. She received her Ph.D. from Andhra University in 2004. She is currently working as professor in Andhra University. She has over 30 years of teaching experience and has published over 86 articles in prestigious international journals. Her areas of interest include artificial intelligence applications to power systems, digital circuits & devices, embedded systems applications, automation, and renewable energy sources. She can be contacted at email: prof.kramasudha@andhrauniversity.edu.in.

Molleti Venkata Pankaj Lahari received B.Tech. in 2013 and M.Tech. in 2015 in electrical & electronics engineering and power electronics & drives respectively, from GVP College of Engineering (Autonomous), Visakhapatnam, India. She received her Ph.D. from Andhra University, India in 2022. She has a teaching experience of six years and research experience of seven years. Her areas of interest are power electronics, electrical drives, real-time modelling & simulation, and embedded systems applications in electrical engineering. She can be contacted at email: laharimolleti14@gmail.com.

Akkapeddi Chandra Sekhar has completed his Ph.D. from JNTU Hyderabad, India in 2008. He is currently working as a professor at Department of Mathematics in GITAM University, Visakhapatnam, India and has over 30 years of teaching experience. He has two patents registered by his name and has published 18 papers in international journals. His areas of interest include algebraic structures in cryptography, mathematical analysis of dynamic systems, and analysis of differential equations. He can be contacted at email: cakkaped@gitam.edu.